

## Response of west India coastal waters and Kavaratti lagoon to the November-2009 tropical cyclone *Phyan*

Antony Joseph<sup>1</sup>, R.G. Prabhudesai<sup>1</sup>, Prakash Mehra<sup>1</sup>, V. Sanil Kumar<sup>1</sup>, K.V. Radhakrishnan<sup>2</sup>, Vijay Kumar<sup>1</sup>, K. Ashok Kumar<sup>1</sup>, Yogesh Agarwadekar<sup>1</sup>, U.G. Bhat<sup>2</sup>, Luis Ryan<sup>1</sup>, Pradhan Rivankar<sup>1</sup>, Blossom Viegas<sup>1</sup>

<sup>1</sup>National Institute of Oceanography, Council of Scientific and Industrial Research,  
Dona Paula, Goa - 403 004, INDIA

<sup>2</sup> PG Center for Marine Biology, Karnataka University, Kodibag, Karwar - 581303  
Karnataka, INDIA

Corresponding author e-mail: [joseph@nio.org](mailto:joseph@nio.org)

**Abstract:** Response of the coastal waters of eastern Arabian Sea (AS) and Kavaratti Island lagoon in the AS to the tropical cyclonic storm 'Phyan', which developed in winter in the south-eastern AS and swept northward along the eastern AS during 9-12 November 2009 until its landfall at the northwest coast of India, is examined based on in-situ and satellite-derived measurements. Wind was predominantly south/south-westerly and the maximum wind-speed ( $U_{10}$ ) of ~16 m/s occurred at Kavaratti Island region followed by ~8 m/s at Dwarka (Gujarat) and ~7 m/s at Diu (located south of Dwarka) as well as two southwest Indian coastal locations (Mangalore and Malpe). All other west India coastal sites recorded maximum wind speed of ~5-6 m/s. Gust-factor (*i.e.*, gust-to-speed ratio) during peak storm event was highly variable with respect to topography, with steep hilly stations (Karwar and Ratnagiri) and proximate thick and tall vegetation-rich site (Kochi) exhibiting large values (~6) whereas Island station (Kavaratti) exhibiting ~1 (indicating consistently steady wind). Rainfall in association with Phyan was temporally scattered, with the highest 24-h accumulated precipitation (~60 mm) at Karwar and ~45 mm at several other west India coastal sites. Impact of Phyan on the west India coastal waters was manifested in terms of intensified significant waves (~2.2 m at Karwar and Panaji), sea surface cooling (~5°C at Calicut), and moderate surge (~50 cm at Verem, Goa). The surface waves were south-westerly and the peak wave period ( $T_p$ ) shortened from ~10-17 s to ~5-10 s during Phyan, indicating their transition from the long-period 'swell' to the short-period 'sea'. Reduction in the spread of the mean wave period ( $T_z$ ) from ~5-10 s to a steady period of ~6 s was another manifestation of the influence of the cyclone on the surface wave field. Several factors such as (i) water piling up at the coast supported by south/south-westerly wind and seaward flow of the excess water in the rivers due to heavy rains, (ii) reduction of piling up at the coast, supported by the upstream penetration of seawater into the rivers, and (iii) possible interaction of upstream flow with river runoff, together resulted in the observed moderate surge at the west India coast. Despite the intense wind forcing, Kavaratti Island lagoon experienced insignificantly weak surge (~7 cm) because of lack of river influx and absence of a sufficiently large land boundary required for the generation and sustenance of wave/wind-driven water mass piling up at the land-sea interface.

**Keywords:** Cyclonic storm 'Phyan', Internet-accessible network, wind, gust, waves, cooling, rainfall, storm surge

## 1. Introduction

In the Indian Ocean rim countries, tropical cyclones rank as the highest cause of loss of lives and property damage related to natural disasters although these regions have been affected several times in the past by earthquakes and recently even tsunamis. Tropical cyclones generate strong wind fields and rainfall. Passage of such cyclones over a large surface of water (such as sea) gives rise to unusually large waves and swells. The cyclone-generated winds cause seawater to pile up on the coast and lead to storm-surge (*i.e.*, inundation and flooding of low-lying coastal regions). Most of the countries located along the periphery of the North Indian Ocean, particularly Bay of Bengal, are threatened by storm surges associated with severe tropical cyclones. The destruction due to the storm surge is a serious concern along the coastal regions of India, Bangladesh, and Myanmar bordering the Bay of Bengal. Although the frequency of storm surges is less in the Arabian Sea (AS) than in the Bay of Bengal (BoB), major destructive surges have occurred at some locations on the eastern boundary of the AS as well, particularly the coasts of Pakistan and Gujarat (India). Monitoring and study of storms and their adverse influences assume greater significance at present in view of several impending dangerous consequences and the resulting altered large-scale atmospheric circulation (e.g., Ulbrich *et al.*, 2009; Meehl *et al.*, 2007). The anticipated consequences include change in cyclone activity in the form of an increase in the frequency and intensity of tropical cyclones as a consequence of increasing greenhouse gases or just a result of natural variability (Goldenberg *et al.*, 2001). In this study, we use remotely sensed wind, wave, and sea surface temperature data as well as in-situ surface meteorological, sea-level, and wave data from spatially distributed west India coastal locations and Kavaratti Island in the eastern AS to examine the effects of the tropical cyclone Phyan at these regions.

## 2. Tropical cyclone *Phyan*: genesis and track

Although cyclonic storms in the Arabian Sea during November are few and far between (the last such storm in November was in 1966), a cyclonic storm, named *Phyan* developed over the south-eastern Arabian Sea during November 2009. According to the records of India Meteorological Department (IMD), a low pressure that formed over Kanyakumari area on 7<sup>th</sup> November 2009, in association with active northeast monsoon surge, became well marked over Lakshadweep Archipelago area over the next one day. By 9<sup>th</sup> noon, the low pressure concentrated into a depression (Fig. 1a) and lay centred over the southeast and the adjoining east central Arabian Sea (Lat: 11.0° N and Long: 72.0° E) in the Lakshadweep Archipelago region. The depression moved initially in a north/north-westerly direction till 10<sup>th</sup> morning, subsequently re-curved north/north-eastwards, and then intensified into a deep depression (Fig. 1b), followed by the formation of a cyclonic storm *Phyan* by the midnight of 10<sup>th</sup> November (Fig. 1c). *Phyan* continued its onward march at varying stages of intensity, finally approaching the west coast of the Indian mainland (Fig. 1d) on 11<sup>th</sup> noon due to its north-eastward movement at a speed of ~20 m/s. The estimated central pressure (ECP) of the system fell from 1000 mb on 9<sup>th</sup> afternoon to 988 mb by 11<sup>th</sup> noon. The sustained maximum wind at surface was estimated to be ~45 knots (~83 km/h) with gust up to 50 knots (92 km/h) for a temporary period during 11<sup>th</sup> morning. The track of *Phyan* during its onward march from 9<sup>th</sup> to 12<sup>th</sup> November (Fig. 2) indicates its initial north-westerly motion from the south-eastern AS along a short segment and the subsequent diversion towards north/north-easterly direction until its landfall and inevitable decay within a short span of time thence. As a result of this cyclonic storm, widespread rainfall and wind flow occurred over Lakshadweep Islands, Kerala, Karnataka, Goa, Konkan, Madhya Maharashtra and south Gujarat region during its evolution and sustenance over a large area on the west India region, stretching from the Arabian Sea toward the

northeast over India's interior, blanketing much of the coast in clouds (Fig. 3). The cyclonic winds in association with *Phyan* left a path of human death (several fishermen) and severe damage to crops and properties (several tens of boats and barges capsized and lost, especially in Goa, Maharashtra, and Gujarat). It provoked a significant disruption of transportation services (road, railway, aircraft, and ship) in the west India coastal sectors and cancellation of air and ship navigation between Lakshadweep group of Islands and the Indian mainland. The timely warnings issued by the India Meteorological Department likely have prevented higher damages and fatalities (e.g., fishing boats at places such as Karwar were berthed in the harbour until the cyclone subsided). Since the 26 December 2004 Indian Ocean tsunami, the cyclonic storm *Phyan* is considered to be the next biggest natural calamity (but considerably lesser in severity relative to the tsunami) that hit the country in recent times, having left a trail of destruction and some human fatalities.

### **3. Data collection schemes**

Data collection required for the present study was accomplished through in-situ and satellite-based measurements. Location map of measurement sites along the west coast of India and from Kavaratti Island region during the passage of tropical cyclone 'Phyan' is indicated in Fig. 4.

#### **3.1 In-situ measurements**

In-situ measurements from the west India coastal stations of Kochi, Malpe, Karwar, Goa, and Ratnagiri as well as Kavaratti Island in the Lakshadweep Archipelago in the south-eastern Arabian Sea were made with the use of an Internet-accessible real/near-real time reporting Integrated Coastal Observation Network (ICON) designed, developed and established by the National Institute of Oceanography (NIO) of India (Prabhudesai et al., 2010), whose output can be viewed at <http://inet.nio.org>. Summary of different instruments used for surface met observations is given in Table 1.

Subsurface pressure sensors and downward-looking aerial microwave radars are incorporated in the sea-level station network. The pressure sensor consists of piezoresistive strain-gauge whose accuracy for water level measurement is  $\pm 1.8$  cm. The accuracy of microwave radar sensor, whose transmission frequency is 24 GHz and operates on time-of-flight principle, is better than  $\pm 1$  cm. Sea-level and surface meteorological parameters (vector-averaged wind speed & direction, gust, barometric pressure, atmospheric temperature, solar radiation, relative humidity, and rainfall) are acquired at 5-, and 10- min intervals, respectively. Installation of sea-level sensors free from the influence of stilling-wells and long narrow tubes renders the measurements ideal for storm-surge studies by preventing under-estimation of large-amplitude short-period signals. In-situ wave measurements were made off Karwar station using a directional wave-rider buoy (Datawell bv, Netherlands). All the sensors used for surface meteorological and sea-level measurements were newly procured ones and therefore calibration was not required.

All the five coastal locations, from which in-situ time-series surface meteorological measurements are available, exhibited barometric pressure drop during the passage of the cyclone. The pressure drop was estimated as the difference of the lowest pressure value during *Phyan* from the average value of the time-series pressure data covering one week before and one week after the passage of *Phyan*. Spatial distribution of barometric pressure drop along these five locations during the passage of the cyclone (Fig. 5) clearly indicates the trend of intensified depression in the northward direction along the coast. The 10- min vector-

Table 1. Summary of different instruments used for surface met observations

<i>Surface meteorological parameters</i>	<i>Sensors</i>	<i>Manufacturer</i>	<i>Range</i>	<i>Accuracy</i>
Wind speed & direction.	Four-blade helecoïd propeller (speed) and light weight vane & precision potentiometer (direction).	RM Young, USA	0-60 m/s	0.2 m/s
Air temperature	Thermistor	YSI, USA	0 - 45°C	± 0.15°C
Barometric pressure	Temperature-compensated piezoresistive strain-gauge pressure transducer.	Honeywell, USA	800 - 1060 mb	0.4 mb
Humidity	Polymer capacitor sensor.	Rotronic, USA	0 - 100 % RH	3 %
Solar radiation	Silicon photodiode with wide spectral response.	Licor, USA	0-300 mW/cm <sup>2</sup>	5%
Rain	Tipping bucket rain gauge with a switch closure for each bucket tip.	RM Young, USA		3%

averaged wind speed and gust values (*i.e.*, the largest wind speed amongst an ensemble of 60 samples that are measured during the 10-minute sampling span) acquired at 10-min sampling interval together with the wind-gust factor (*i.e.*, gust-to-speed ratio) shows the gusty nature of the wind regime during the cyclone. Only the wind speeds  $\geq 1$  m/s have been considered for estimation of gust-factor so that unrealistically over-estimated gust-factor values arising from the use of negligibly small wind speeds are inhibited.

Spatial distribution of gust maxima (Fig. 6a) indicates the distinctively large gusty nature of wind at Ratnagiri (~30 m/s) during the currency of Phyan in contrast to the considerably smaller gust (10-14 m/s) observed at all the other stations considered in the present study. Interestingly, the gust factor maxima (Fig. 6b) indicate a different trend in which while Karwar and Ratnagiri topped the gust-factor maxima (~6) followed by Kochi (~5), Malpe and Dona Paula (Goa) exhibited the least gust factor (~4). Stick-plots of the wind velocities at these coastal

regions (Fig. 7) indicate the predominantly south/south-westerly and south/south-easterly wind field at most of these locations during Phyan. Rainfall data available from Kochi (in the south) and the Konkan regions (covering Malpe, Karwar, Goa, and Ratnagiri) during November provide an indication of the spatial distribution of the unusually large precipitation level (*i.e.*, 24-h cumulative rainfall) at these stations in association with the Phyan (Fig. 8). It is seen that Karwar stands out distinctively as a region which experienced the largest rainfall in contrast to its neighbouring coastal regions during the cyclonic storm. Kochi region experienced the least amount of rainfall during the cyclonic storm. Atmospheric cooling and spatial distribution of air temperature drop (Fig. 9) along five west India coastal regions in association with the tropical cyclonic storm indicate that the proximate regions of Malpe, Karwar and Dona Paula (Goa) experienced the maximal cooling.

In-situ time-series measurements of significant wave height, wave direction, and wave period were made off Karwar using directional wave rider buoy (See Fig. 10). These measurements indicate the response of the sea in terms of abrupt rise in significant wave height in association with the cyclone. The surface waves were south-westerly and the peak wave period ( $T_p$ ) shortened from  $\sim 10$ -17 s to  $\sim 5$ -10 s during Phyan, indicating their transition from the long-period 'swell' to the short-period 'sea'. Reduction in the spread of the mean wave period ( $T_z$ ) from  $\sim 5$ -10 s to a steady period of  $\sim 6$ s was another manifestation of the influence of the cyclone on the surface wave field. The surge generated at the west-India coastal locations during the passage of Phyan was moderate (Fig. 11).

Installation of a new surface meteorological station (NIO-AWS) at Katchery jetty in the Kavaratti lagoon a few days prior to the occurrence of Phyan provided a fortuitous opportunity to examine the surface meteorological features at this region in association with the cyclonic storm. In-situ measurements (Fig. 12) indicate the intensified winds (Fig. 12a, d) and barometric pressure drop (Fig. 12g) that developed over this island in the Lakshadweep Archipelago and its proximate regions in the eastern AS. However, no discernible atmospheric temperature drop was indicated (Fig. 12f). The predominant wind field at Kavaratti region in association with Phyan was south-westerly, which is in agreement with the wind data at all the west India coastal sites. An interesting observation is the insignificant gust-factor ( $\sim 1$ ) during the passage of Phyan, which is distinctly at variance with the usually large gust-factor ( $\sim 3$ -4) at this site during normal weather conditions (See Fig. 12b). A downward-looking microwave radar gauge installed by NIO at Katchery jetty provided sea-level measurements at 5-minutes interval. The observed surge maximum was  $\sim 10$  cm (Fig. 12h).

### 3.2 Satellite-derived measurements

Satellite-derived measurements used in the present study are wind velocity, significant wave height, and sea surface temperature. Surface-wind speed and direction data used for the analysis were obtained from AVISO (<http://www.aviso.oceanobs.com>) and QuikSCAT ([http://www.ssmi.com/tmi/tmi\\_browser.html](http://www.ssmi.com/tmi/tmi_browser.html)). Significant wave data were obtained from AVISO. Wind and significant wave height were derived from a dual-frequency Ku/C band Solid State Radar Altimeter (Poseidon-2) CNES on the JASON-1 satellite altimeter mission, operating at 13.575 GHz (Ku band) and 5.3 GHz (C band). At the satellite data processing centre, the measurements made at these two frequencies are combined to obtain measurements of the wind speed and significant wave height with correction for the influence of the ionosphere on the altimeter signals (AVISO and PODAAC User Handbook, IGDR and GDR Jason products, CNES and NASA, Edition 4.1, October 2008). At this centre, the altimeter wind speed is estimated through a mathematical relationship with the Ku-band backscatter coefficient and the significant wave height using the Vandemark and Chapron algorithm. The wind speed model function is evaluated for 10 m above

the sea surface ( $U_{10}$ ) and is considered to be accurate to 2 m/s. SST data (derived from satellite microwave radiometer) were obtained from TRMM Microwave Imager [TMI] instrument mounted on the platform of NASA's Tropical Rainfall Measuring Mission satellite ([http://www.ssmi.com/tmi/tmi\\_browser.html](http://www.ssmi.com/tmi/tmi_browser.html)). Inter-comparison studies by Gentlemann and Wentz (2001) of TMI SSTs with buoy SSTs found that the former are in excellent agreement with the latter, with a standard deviation of  $0.52^{\circ}\text{C}$  and a mean bias of  $-0.13^{\circ}\text{C}$ . Whereas QuikSCAT and TMI data are in binary format, AVISO data are in ASCII format. In the present study, time-series data from a given location pertaining to every parameter derived from satellite-borne sensors were available at a frequency of 1 sample per day.

Satellite-derived vector plots of the wind-field over the eastern AS during the passage of the tropical cyclonic storm Phyan in November 2009 illustrates the spatial structure and vortex motion of the wind field (Fig. 13). Because of limited in-situ measurement locations, sea-surface wind ( $U_{10}$ ), sea-surface waves (significant wave height, wave direction, wave periods), and sea surface temperature (SST) were extracted from remotely sensed satellite-derived measurements from a chain of selected locations (See Fig. 4). Satellite-derived time-series of wind speed from twelve west India coastal water locations during the passage of the cyclonic storm indicate that the maximum wind-speed ( $U_{10}$ ) of 8 m/s occurred at Dwarka in Gujarat, followed by  $\sim 7$  m/s at Diu (located just south of Dwarka) as well as two southwest Indian coastal locations (Mangalore and Malpe). All other western coastal Indian locations recorded the maximum wind speed of  $\sim 5$ -6 m/s. Spatial distribution of the wind speed maxima along twelve west India coastal sites during the passage of *Phyan* (Fig. 14) provides an indication of the gradual intensification of wind speed maxima from the south-western region of India until Mangalore region followed by its gradual weakening from Mangalore region to Ratnagiri region, and its subsequent renewed intensification from Ratnagiri region until the Gujarat coast of the north-eastern AS. Since in-situ measurement of significant wave height from a wave rider buoy was available from a location off Karwar during the passage of Phyan (See Fig. 10), these measurements were used to calibrate the satellite-derived significant wave height measurements. It was found that at Karwar the latter was 1.42 times larger than the former, because of which a correction factor of  $1/1.42$  was applied to the satellite-derived significant wave height measurements to match them with in-situ measurements. This correction factor was then applied to the satellite-derived significant wave height measurements from all other locations. Time-series measurements indicate that the maximum significant wave height of 2.2 m occurred at Karwar (Karnataka State) and Panaji (Goa State), followed by 1.9 m at Ratnagiri (Maharashtra State) and  $\sim 1.5$  m at all other west India coastal regions (Fig. 15). This shows the larger sensitivity/tendency of Karwar (Karnataka) and Panaji (Goa) regions to sea surface wave intensification, followed by Ratnagiri in Maharashtra. The Phyan caused sea surface cooling as demonstrated from a drop in SST in several regions. However, SST at Kanyakumari region, where a low pressure area formed on 7<sup>th</sup> November 2009 in association with the cyclone genesis, did not reveal a noticeable cooling effect. As evidenced from the spatial distribution of SST drop along the west India coastal waters during the passage of the cyclone (Fig. 16), the largest sea surface cooling occurred at Calicut and the smallest at Kanyakumari and Porbander.

#### **4. Discussion of results**

To a first order approximation, the spatial pressure gradient associated with a cyclone primarily determines the storm-related wind field. According to the existing notion, the largest wind speeds occur in the areas where the passing cyclone further tightens the ambient pressure gradients. Such forcing across the seawater regions

generates intensified sea surface waves, water currents, storm surges and associated low-land inundation, and under supportive circumstances gives rise to up-welling in the sea which together with evaporative cooling results in enhanced sea surface cooling. As indicated by Uccellini (1990), forcing factors of cyclogenesis interact nonlinearly, over small areas, or over a limited period during the storm development.

#### **4.1 Atmospheric pressure gradient and winds**

The passage of Phyan was associated with a well-marked barometric pressure drop, whose spatial distribution (Fig. 5) clearly indicates its intensification in the northward direction along the coast (See Fig. 4 for location map). The cyclonic storm, which could have primarily been the result of the strengthened synoptic scale pressure gradient, was found to be associated with unusually large surface winds and gusts. The observed strong variability of wind gusts (See Fig. 6a) could be associated with a downward mixing of upper-level higher wind speeds to the surface and/or the lateral spreading of convective downdrafts caused by evaporating rain in the convective storms. These observations imply that the maximum gust could be a result of a destabilization of the lower troposphere during the passage of Phyan. Unfortunately, no upper-air soundings during the passage of the cyclone are available to corroborate this inference. A closer examination of Fig. 6 reveals a strong station-to-station variability with respect to the maximum observed winds and gusts during the passage of the cyclone. The gust-factor provides a quantitative measure of the gustiness of the wind field (*i.e.*, wind occurring in pulses rather than in a steady fashion). It is found that during Phyan the gust-factor differed considerably from station to station. For example, whereas Karwar and Ratnagiri registered gust-factor of ~6 and Kochi ~5, Malpe and Goa registered a lower value (~4). Gust-factor at Kavaratti Island during peak winds is <2 (See Fig. 12). Both Ratnagiri and Karwar, which witnessed the largest gust-factor, are stations located on sharply steep hills. However, Malpe and Kochi are coastal plane areas and Kavaratti is a small island in the open sea. Dona Paula is neither plane nor a steep hilly location. From the above description it is found that the gust-factor during peak storm event is highly variable with respect to topography, with steep hill stations exhibiting the largest value whereas coastal planes and Island station exhibiting the least. However, Kochi station located right on the beach and the periphery of Kochi backwaters, exhibiting a fairly large gust factor (~5) during peak cyclone winds is a contradiction. Perhaps, the presence of thick vegetation in the vicinity of the measurement site must have contributed in some way to the observed fairly large gust-factor at this station. As noted by Fink *et al.* (2009), these results could be indicative of the considerable influence of macro-meteorological (*i.e.*, orography) or micro-meteorological (*i.e.*, trees, buildings, etc.) environmental conditions of the stations on the gust-factor, a peculiarity observed only during storm conditions.

#### **4.2 Precipitation and atmospheric cooling**

Fast sampled (10-min sampling interval) in-situ measured rainfall data available from a few locations allowed examination of the spatial characteristics of the cyclone-induced rainfall distribution. The rainfall associated with Phyan was temporally scattered, with the highest value of 24-h accumulated precipitation observed at Karwar (60 mm); followed by Ratnagiri, Dona Paula and Malpe (~45 mm); and the least at Kochi (~37 mm). However, torrential rain was absent at all the locations. As the cyclone storm moved forward approximately in the northward direction and inclined towards the west India coast, arrival of the cyclone-associated rainfall also followed this pattern, occurring first at the southern region and subsequently at the next northern locations. Although November falls under the Indian winter monsoon period, rainfall was totally absent at these stations during the few days preceding

the cyclone. The temporal and spatial distribution of the 24-h accumulated cyclone-associated rainfall (Fig. 8), with the hill-dominated stations receiving substantially more rainfall, provides an indication that the amount and distribution of rainfall depends not only on the distribution of convection within the cyclone but also on orographic lifting effects. Distribution of convection and rainfall in a tropical cyclone has certain characteristic patterns both when it is over open ocean (Lonfat *et al.*, 2004) and when making landfall (Chan *et al.*, 2004). Abundant moisture supply, resulting from the proximity of these stations to the cyclone track could be another reason for the substantially enhanced rainfall at these stations. Similar inferences have been drawn by Cheung *et al.* (2008) with reference to the characteristics of rainfall during tropical cyclones in Taiwan. Additionally, the strong precipitation may have been a factor further increasing the wind damage loss in terms of trees fell as a combined result of wind forcing and decrease of the binding strength of soil because of frequent precipitation. The precipitation triggered by the cyclonic storm gave rise to atmospheric cooling of  $\sim 3.5^{\circ}\text{C}$  (Fig. 9).

### **4.3 Significant wave height intensification**

The activated surface wind speed in association with Phyan caused intensified sea surface wave conditions all along the west India coastal waters (Fig. 15). The highest significant wave height of 2.19 m occurred at Karwar and Panaji, followed by Ratnagiri with 1.87 m. All other locations exhibited  $\sim 1.5$  m significant wave height. It may be noted that coastal water regions of the sea are characterized by complex geometry (bathymetry, shape of land-sea interface, etc) and dynamics (e.g., current pattern), all of which may play a role in the sea surface wave characteristics. It is known that like any other waves, the ocean waves suffer refraction and reflection because of region-specific influences such as changes in bathymetric slope, coastal alignment relative to the direction of arrival of wave front, and peculiarities of the coastal contour. These influences give rise to convergence of waves at one region and divergence at another. Such convergence during certain weather conditions are known to generate concentration of wave energy at specific areas through focussing (Kjeldsen, 1991). Karwar, Panaji, and Ratnagiri regions (offshore of which the maximum significant wave heights were observed) have corrugated coastal topography. Wave focusing and amplification by the curvature of the land-sea interface could be a particularly important factor that influences the wave heights at these coastal water bodies.

It is known that water currents can amplify ocean waves by refraction-dominated wave-current interaction. Waves in combination with strong current shear and local topography (bathymetry) give rise to locally amplified wave zones in some areas [e.g., Vesecky and Stewart, 1982; Irvine and Tilley, 1988]. In the present study, Karwar and Panaji are qualified by the outfall from the Kali River and Mandovi-Zuari estuarine network, respectively. It is quite reasonable that the observed relatively larger wave heights at these two coastal water bodies might have been caused by the wave-current interaction driven by the strong precipitation-induced downstream freshwater discharge currents from these rivers.

### **4.4 Sea surface cooling**

Phyan caused drop in SST at several coastal water regions, with the largest drop ( $5.5^{\circ}\text{C}$ ) at Calicut and the smallest at Kanyakumari and Porbander (Fig. 16). Some of the reasons for the observed drop in SST during the passage of the cyclone could be surface cooling due to evaporation and up-welling, arrival of cooler subsurface water to the surface as a result of the stirring of the upper ocean layers by the high winds associated with the cyclone or removal of heat from the ocean surface through the action of vertical redistribution of heat. The cyclone-



driven surface wind near Calicut region was  $\sim 5$  m/s and this must have in part given rise to the observed sea surface cooling. However, whereas the atmosphere tends to respond almost instantaneously, the sea is expected to react more slowly due to its high heat capacity. Intensification of sea-surface wave climate could also influence sea surface cooling in part through increased mixing. However, Calicut, where the largest drop in SST occurred, is a region where the wave climate was weaker (See Fig. 15), relative to that at other regions such as Karwar, Panaji and Ratnagiri where the significant wave heights were larger. One of the plausible reasons for the observed relatively larger cooling at Calicut could be the presence of internal waves, which play an important role in ocean mixing processes. Such slow speed waves are found in all oceans in the thermocline region, in regions of strongly sheared currents (Boyd et al., 1993), gulfs (Munk, 1941), straits (Shand, 1953), most bays, and even in shallow waters (Lee, 1961), and vary widely in amplitude, period, and depth (Garrett and Munk, 1975). However, time-series in-situ measurements to substantiate the presence of internal waves off Calicut during Phyan are not available. Thus, a variety of presently unknown factors such as precipitation- or wind-induced atmospheric cooling, up-welling, internal waves etc., individually or in combination appear to have given rise to the observed sea surface cooling.

#### 4.5 Storm surge

An above-normal sea-level rise caused by strong tropical storm, known as storm surge, results from strong winds, atmospheric pressure disturbances, rainfall, and intensified sea surface waves and swells associated with the storm. The storm parameters that determine the coastal surge level are the storm characteristics such as (1) central pressure ( $c_p$ ), (2) storm size (*i.e.*, radius of maximum wind speed [ $R_{max}$ ]), (3) storm forward velocity [ $v_f$ ], (4) inclination of storm track relative to the coast ( $\theta$ ), (5) landfall location, as well as the storm-wind fields. The rate of change in  $c_p$  is reasonably linearly dependent on storm size. Major storms tend to be stronger off the coast and begin to decay before they make landfall, the quantum of decay being site-specific to a given area. The wind fields in cyclones vary considerably during their approach to the shore. Extensive numerical studies have shown that coastal surge levels are very sensitive to storm intensity, typically categorized by pressure differential defined as the peripheral pressure minus central pressure (*i.e.*,  $\Delta p = p_0 - c_p$ , where  $p_0$  is the peripheral pressure), storm size (*i.e.*,  $R_{max}$  or  $R_p$ ), and storm location relative to a site. However, based on the results of sensitivity studies, storm surge is less sensitive to  $\theta$  and  $v_f$  (during approach to land). It has been reported that characteristic variations of coastal surges as a function of  $\Delta p$ ,  $\theta$ , and  $v_f$  tend to be quite smooth with either linear or slightly curved slopes (Resio, *et al.*, 2009). For a given location, a major portion of the surge response to the cyclone is captured by the variation of  $\Delta p$  and  $R_p$  (Irish *et al.*, 2008).

The total coastal sea-level elevation is the combined effect of storm surge, wave set-up, and tidal elevation; together with the non-linear interaction of wind-waves and tides with the storm surge. Locally generated seiches can also contribute elevation changes of order 1 m at some stations. As observed by Johns *et al.*, (1985) and more recently by Sinha *et al.*, (1996; 2008), the non-linear interaction of surge and tide may significantly modify the evolution of surges. However, based on numerical experimental results, it has been reported that although there may be some degree of nonlinearity in the superposition of tides and storm surges, linear superposition provides a reasonable estimate of the (nonlinearly) combined effects of tides and surges (Resio *et al.*, 2009). Except the southern peninsular region, the west India coastal waters are tidally dominated. Following

conventional practice, we first decomposed the instantaneous sea level ( $\eta$ ) into a tidal ( $\eta_T$ ) and residual ( $\eta_R$ ) component, so that  $\eta = \eta_T + \eta_R$

Tide is deterministic, and given its harmonic constants, it is readily predictable for any period. The residual includes all types of sea-level contributions which are non-tidal (e.g., storm surges, harbour seiches, etc.). In general, there exists a transfer function between atmospheric forcing and the sea-level response. The observed surge heights at the coastal locations considered in the present study are in agreement with the barometric pressure drop, with the larger surge corresponding to the larger pressure drop (See Figs 5 and 11). Also, both Karwar and Verem (Panaji/Dona Paula, Goa), which experienced the largest significant wave height, exhibited the largest surge (See Figs. 11 and 15) thereby indicating the role of wave set-up in the surge generation at these locations. Analysis of surges associated with hurricanes *Katrina* and *Rita* provided convincing indications that waves contribute significantly to coastal surges (Resio *et al.*, 2009) primarily because of wave-driven water mass transport (Longuet-Higgins, 1953) and radiation stress from wave fields (Longuet-Higgins and Stewart, 1964). Other factors that influence coastal surges are wave-current interactions, coastal bathymetry and landforms.

The evolution of storm surges near the coast is known to be very sensitive to the coastal geometry and offshore bathymetry. This is seen in our measurements from several locations during Phyan. The wind at the west India coastal waters during Phyan was south/south-westerly, thus possessing a landward-oriented cross-shore component and a north-pole-ward oriented alongshore component, both of which supports piling up of water on the west India coast (the latter being by virtue of Coriolis force trying to deflect the water mass to the east because of India's position in the Northern Hemisphere). Thus, the effective wind-driven surge at this coast is a manifestation of these two supporting effects if the land-sea interface is continuous (*i.e.*, devoid of breaks). In the present study Malpe, Karwar, and Goa, which are the three coastal locations from which sea-level measurements are available, are estuarine sites which communicate with the Arabian Sea. These estuaries have given rise to breaks in the coast, thereby providing an additional path for the water to escape into the river, instead of getting piled up. However, these estuaries also provide the requisite pathways for the discharge of appreciable quantity of fresh water supplied by the heavy precipitation associated with the cyclone and carried by the rivers into the sea. Further, since the regions under the present study fall under the influence of freshwater runoff from major rivers and river systems, the influx brought by them operates as a buoyancy input which influences the baroclinic effects and therefore impacts the surge. Although the rainfall at Karwar during Phyan was larger than that at Goa, the latter witnessed the largest surge because the combined river discharge there from two larger rivers (Mandovi and Zuari) was much larger than that at Karwar from a relatively small single river (Kali). Thus, the combinations of several opposing effects have contributed to the evolution of the observed surges on the west India coast in response to Phyan.

The observed surge at Kavaratti Island lagoon was weak ( $\sim 7$  cm). It may be noted that during the passage of Phyan over Lakshadweep archipelago, it was classified as a depression ([www.imd.gov.in](http://www.imd.gov.in)). The surge expected due to inverted barometer effect, at the rate of 1 cm rise in local sea-level per 1 mb drop in local atmospheric pressure (Pugh, 1987) is close to the observed surge. However, during this time the wind and gust at Kavaratti lagoon was consistently large ( $\sim 18$  m/s) and, therefore, generation of a larger surge due to piling up is logically expected. But this is not seen in the measurements and the reasons for which need to be explored. Two reasons that can be attributed to the observed weak surge at Kavaratti lagoon are (i) lack of river influx and (ii) absence of a

sufficiently large land boundary required for the generation and sustenance of water mass piling-up at the land-sea interface as a result of wave/wind-driven water mass transport.

Question could justifiably be posed as to why the 26 December 2004 Indian Ocean tsunami (IOT) generated surge at this island despite the absence of a large land boundary. To answer this question, the geography of Kavaratti Island and its surrounding seafloor features as well as the response of tsunami waves to such features need to be taken into account. For this purpose, it is to be recognized that Kavaratti Island is not just an isolated piece of land protruding out from the Arabian Sea, but an intricate entity of a conglomeration of islands and sea mount chains in the Lakshadweep Archipelago, which, in turn, are extensions of a much larger geographical entity consisting of the Maldives Islands and sea mount chains of varying heights and lengths associated with them (See the seafloor features indicated in Fig. 2). According to the presently available knowledge based on global measurements of the December 2004 Indian Ocean tsunami which penetrated all the oceans, tsunami is a series of waves that penetrate the entire water depth; and propagating at high speed with a coherent elevation and depression of large expanses of the ocean surface within the wave (Joseph, 2010). The tsunami waves are obstructed and modified not only by the physical boundary at the air-land-sea interface but also by continental shelves, ridges, and seamount/island chains (Titov et al., 2005; Kowalik *et al.*, 2005; Kowalik *et al.*, 2006; Joseph *et al.*, 2006; Kowalik et al., 2007; Candella et al., 2008; Kowalik et al., 2008; Tanioka et al., 2008). Evidence for local amplification of tsunami waves by a ridge is provided by Rabinovich and Thomson (2007). Pattiaratchi and Wijeratne (2009) have demonstrated the influence of Maldives Island chain on tsunami propagation. Thus, the entire island chain including the sea mounts and other submarine topographic structures located in between them (rather than Kavaratti Island alone) together functions as a single physical boundary to facilitate surge generation at this island in response to the tsunami waves. It is known that submarine topographic structures function as tsunami wave guides (Marchuk, 2009), as a result of which tsunami wave energy gets amplified, trapped and ducted by them. In contrast, wind forcing is primarily a surface phenomenon and, therefore, the mechanism required for the piling-up to happen is a sufficiently long/broad/tall land-sea boundary above the sea-surface. Consequently, subsurface topographic features have hardly any role to contribute to surge resulting from wind-induced piling-up effect. On this basis, absence of a sufficiently large land boundary at Kavaratti Island can reasonably be considered to be primarily the reason for the observed weak surge at Kavaratti lagoon despite strong winds experienced there in association with Phyan. Thus, generation of a larger surge at Kavaratti Island in response to the 26 December 2004 Indian Ocean tsunami cannot be construed as a basis to expect the generation of a larger surge at this island in response to Phyan.

## **5. Conclusions**

The present study is aimed at providing an insight on the synoptic evolution and some meteorological and oceanographic impacts of the cyclonic storm Phyan, which swept approximately in a predominantly north/north-eastward direction along the eastern Arabian Sea between 9 and 12 November 2009 and caused considerable fatalities and economic/environmental damage along the west India coastal and offshore waters. The cyclonic storm Phyan was attended by strong winds and gusts, atmospheric pressure disturbances, intense rainfall, and atmospheric cooling at several regions. It was found that atmospheric forcing exerted considerable influence on sea-level in terms of intensified sea surface waves and increased coastal surge levels. The observed surge heights at the coastal locations considered in the present study are in broad agreement with the barometric pressure drop

(with the larger surge corresponding to the larger pressure drop), discharge of appreciable quantity of fresh water supplied by the heavy precipitation and carried by the rivers into the sea, as well as coastal wave-setup generated by intensified wave height. Other factors that influenced coastal surges are coastal bathymetry and landforms, and possibly even wave-current interactions. Thus, the combinations of several factors such as (i) water piling-up at the coast supported by south/south-westerly winds and waves as well as excess river discharge into the sea (due to heavy rains), (ii) reduction in piling-up at the coast due to the upstream penetration of seawater into the rivers, and (iii) possible interaction of upstream flow with river runoff, together resulted in the observed surge flooding at the west India coast under the influence of Phyan. Despite the intense wind forcing, Kavaratti Island lagoon experienced insignificantly weak surge (~7 cm) because of lack of river influx and absence of a sufficiently large land boundary.

## References

1. Boyd, T.J., S.D. Luther, R.A. Knox, and M.C. Hendershott (1993), High frequency internal waves in the strongly sheared currents of the upper equatorial Pacific: Observations and a simple spectral model, *J. Geophys. Res.*, **98**, 18089-18108.
2. Candella, R.N., A.B. Rabinovich, and R.E. Thomson (2008), The 2004 Sumatra tsunami as recorded on the Atlantic coast of South America, *Adv. Geosci.*, **14**, 117-128.
3. Chan, J.C.L, K.S. Liu, S.E. Ching, and E.S.T. Lai (2004), A symmetric distribution of convection associated with tropical cyclones making landfall along the South China coast, *Mon. Weather Rev.*, **132**, 2410-2420.
4. Cheung, K.K.W, L.-R. Huang, and C.-S. Lee (2008), Characteristics of rainfall during tropical cyclone periods in Taiwan, *Nat. Hazards Earth Syst. Sci.*, **8**, 1463-1474.
5. Fink, A.H., T. Brucher, V. Ermert, A. Kruger, and J.G. Pinto (2009), The European storm Kyrill in January 2007: synoptic evolution, meteorological impacts and some considerations with respect to climate change, *Nat. Hazards Earth Syst. Sci.*, **9**, 405-423.
6. Garrett, C., and W. Munk (1975), Space-time scales of internal waves: A progress report", *J. Geophys. Res.*, **80**, 291-297.
7. Gentlemann, C.L., and F.J. Wentz (2001), Satellite microwave SST: Accuracy, comparison to AVHRR and Reynolds SST, and measurement of diurnal thermocline variability, *Proc. International Geoscience and Remote Sensing Symposium (IGARSS '01), IEEE 2001 International*, Sydney, NSW, Australia, 9-13 July 2001; Vol. 1, pp. 246-248 (Also at <http://ieeexplore.ieee.org>)
8. Goldenberg, S.B., C.W. Landsea, A.M. Mestas-Nunez, and W.M. Gray (2001), The recent increase in Atlantic hurricane activity: Causes and implications, *Science*, **293**, 474-479.
9. Irish, J.L., D.T. Resio, and J.J. Ratcliff (2008), The influence of storm size on hurricane surges, *J. Phys. Oceanogr.*, **38**, 2003-2013.
10. Irvine, D.E and D.G. Tilley (1988), Ocean wave directional spectra and wave-current interaction in the Agulhas from the Shuttle Imaging Radar-B synthetic aperture radar, *J. Geophys. Res.*, **93**(C12), 15389-15401.
11. Johns, B., A.D. Rao, S.K. Dube, and P.C. Sinha (1985), Numerical modeling of the tide surge interaction in the Bay of Bengal, *Philos. Trans. R. Soc. Lond.*, **A 313**, 507-535, doi:10.1098/rsta.1985.0002.

12. Joseph, A., J. T. Odamey, E. K. Nkebi, A. Pereira, R. G. Prabhudesai, P. Mehra, A. B. Rabinovich, V. Kumar, S. Prabhudesai, and P. L. Woodworth (2006), The 26 December 2004 Sumatra tsunami recorded on the coast of West Africa, *African J. Marine Sci.* **28**(3&4), 705-712.
13. Joseph, A. (2010), Tsunamis: Detection, monitoring, and early-warning technologies, *Elsevier Science*, Academic Press, New York (in press).
14. Kjeldsen, S.P (1991), The practical value of directional ocean wave spectra, *Directional Ocean Wave Spectra*, The Johns Hopkins Studies in Earth and Space Sciences, R.C. Beal (Ed), pp. 13-19.
15. Kowalik, Z., W. Knight, and P. Whitmore (2005), Numerical modeling of the global tsunami: Indonesian tsunami of 26 December 2004, *Sci. Tsunami Hazards*, **23**(1), 40-56.
16. Kowalik, Z., W. Knight, T. Logan, and P. Whitmore (2006), Numerical modeling of the Indian Ocean tsunami, In: *The Indian Ocean Tsunami*, (Eds) Murthy, T.S.; Aswathanarayana, U.; Nirupama, N., Taylor and Francis; London; UK; 2006; 97-122.
17. Kowalik, Z., W. Knight, T. Logan, and P. Whitmore (2007), The tsunami of 26 December 2004: Numerical modeling and energy considerations, *Pure Appl. Geophys.*, **164**, 379-393.
18. Kowalik, Z., J. Horillo, W. Knight, and T. Logan (2008), The Kuril Islands tsunamis of November 2006: Part I: Impact at Crescent city by distant scattering, *J. Geophys. Res.*, **113**, C01020.
19. Lee, O.S (1961), Observations on internal waves in shallow water, *Limnology and Oceanography*, **6**(3), 312-321.
20. Lonfat, M., F.D. Marks Jr., and S.S. Chen (2004), Precipitation distribution in tropical cyclones using the Tropical Rainfall Measuring Mission (TRMM) microwave imager: A global perspective, *Mon. Weather Rev.*, **132**, 1645-1660.
21. Longuet-Higgins, M.S (1953), Mass transport in water waves, *Philosophical Transactions of the Royal Society of London*, **245**, 535-581.
22. Longuet-Higgins, M.S., and R.W. Stewart (1964), Radiation stresses in water waves; a physical discussion, with applications, *Deep-Sea Res.*, **11**, 529-562.
23. Marchuk, A. G (2009), Tsunami wave propagation along waveguides, *Science of Tsunami Hazards*, **28**(5), 283-302.
24. Meehls, G.A., T.F. Stocker, W.D. Idlingstein, A.T. Gaye, J.M. Gregory, A. Kitoh, R. Knutti, J.M. Murphy, A. Noda, S.C.B. Raper, I.G. Watterson, A.J. Weaver, and Z.-C. Zhao (2007), *Climate change: The physical science basis*, United Kingdom and New York, NY, USA, Cambridge University Press, Chap. Global Climate Projections.
25. Munk, W.H (1941), Internal waves in the Gulf of California, *J. Marine Res.*, **4**, 81-91.
26. Pattiaratchi, C.B., and E.M.S. Wijeratne (2009), Tide gauge observations of 2004-2007 Indian Ocean tsunamis from Sri Lanka and Western Australia, *Pure appl. Geophys*, **166**, 233-258.
27. Prabhudesai, R.G., A. Joseph, Y. Agarwadekar, P. Mehra, K. V. Kumar, and L. Ryan (2010), Integrated Coastal Observation Network (ICON) for real-time monitoring of sea-level, sea-state, and surface-meteorological data, OCEANS' 10 – IEEE Seattle Technical Conference; September 2010; IEEE, 9 pp.

28. Pugh, D. T. (1987), Tides, surges and mean sea-level: A handbook for engineers and scientists (Wiley, Chichester), 472 pp.
29. Rabinovich, A. B., and R. E. Thomson (2007), The 26 December 2004 Sumatra tsunami: Analysis of tide gauge data from the World Ocean — Part 1. Indian Ocean and South Africa, *Pure and Applied Geophysics*, **164** (2-3), 261-308.
30. Resio, D.T., J. Irish, and M. Cialone (2009), A surge response function approach to coastal hazard assessment — part 1: basic concepts, *Nat. Hazards*, **51**, 163-182. DOI:10.1007/s11069-009-9379-y.
31. Shand, J.A (1953), Internal waves in Georgia Strait, *Trans. Amer. Geophys. Union*, **34**, 849-856.
32. Sinha, P.C., Y.R. Rao, S.K. Dube, and A.D. Rao (1996), Numerical investigation of tide-surge interaction in Hooghly Estuary, India, *Mar. Geod.*, **19**, 235-255, doi:10.1080/01490419609388082.
33. Tanioka, Y., Y. Hasegawa, and T. Kuwayama (2008), Tsunami waveform analyses of the 2006 underthrust and 2007 outer-rise Kuril earthquakes, *Adv. Geosci.*, **14**, 129-134.
34. Titov, V., A. B. Rabinovich, H. O. Mofjeld, R. E. Thomson, and F. I Gonzalez (2005), The global reach of the 26 December 2004 Sumatra tsunami, *Science*, **309**, 2045-2048.
35. Sinha, P.C., I. Jain, N. Bhardwaj, A.D. Rao, and S.K. Dube (2008), Numerical modeling of tide-surge interaction along Orissa coast of India, *Nat. Hazards*, **45**, 413-427, doi:10:1007/s11069-007-9176-4.
36. Ulbrich, U., G.C. Leckebusch, and J.G. Pinto (2009), Cyclones in the present and future climate: a review, *Theor. Appl. Climatol.*, published online, doi:10.1007/s00704-008-0083-8
37. Uccellini, L.W (1990), Process contributing to the rapid development of extratropical cyclones, In: Extratropical cyclones: The Eric Palmen memorial volume, edited by: Newton, C., and E. Holopainen, *Am. Meteorol. Soc.*, 81-107.
38. Vesecky, J.F., and R.H. Stewart (1982), The observation of ocean surface phenomena using imagery from the SEASAT synthetic aperture radar: An assessment, *J. Geophys. Res.*, **87**(C5), 3397-3430.

## Figures

1. INSAT Kalpana I satellite imageries of cyclonic storm *Phyan* at different stages of intensity (from IMD Report, November 2009).
2. Track of cyclonic storm *Phyan* during 09-12 November 2009 (from IMD Report, November 2009).
3. NASA's Aqua satellite imagery of the spatial coverage of cyclonic storm *Phyan* (November 2009) over a large area on the west India region, stretching from the Arabian Sea toward the northeast over India's interior, blanketing much of the coast in clouds (Courtesy of National Aeronautics and Space Administration, USA).
4. Location map of measurement sites along the west coast of India and from Kavaratti Island region during the passage of tropical cyclone '*Phyan*'.
5. Spatial distribution of barometric pressure drop along five west India coastal locations during the passage of *Phyan*
6. Spatial distribution of [a] gust maxima and [b] gust factor maxima along five west India coastal locations during the passage of *Phyan*
7. Stick-plots of wind velocities at five west India coastal locations during the passage of *Phyan* during November 2009.
8. Spatial distribution of 24-h cumulative rainfall maxima along five west India coastal waters during the passage of *Phyan*
9. Spatial distribution of air temperature drop along five west India coastal locations during the passage of *Phyan*
10. Time series measurements of significant wave height, wave direction, peak wave period ( $T_p$ ) and mean wave period ( $T_z$ ) from Karwar made using directional wave rider buoy.
11. Spatial distribution of surge maxima along three west India coastal locations during the passage of *Phyan*
12. In-situ measurements of the surface meteorological and storm surge features at the Kavaratti Island during the passage of *Phyan*; (a) wind speed and gust; (b) gust factor; . Wind speeds  $\geq 1$  m/s have been considered for estimation of gust factor; (c) wind direction; (d) stick plot of wind velocity; (e) scatter plot of wind speed; (f) air temperature; (g) air pressure; (h) surge.
13. Spatial structure and vortex motion of the wind field over the eastern Arabian Sea during the passage of *Phyan* (QuikSCAT satellite-derived vector plots)
14. Spatial structure and vortex motion of the wind field over the eastern Arabian Sea during the passage of *Phyan* (QuikSCAT satellite-derived vector plots)
15. Spatial distribution of significant wave height maxima along twelve west India coastal locations during the passage of *Phyan*.
16. Spatial distribution of SST drop along twelve west India coastal locations during the passage of *Phyan*

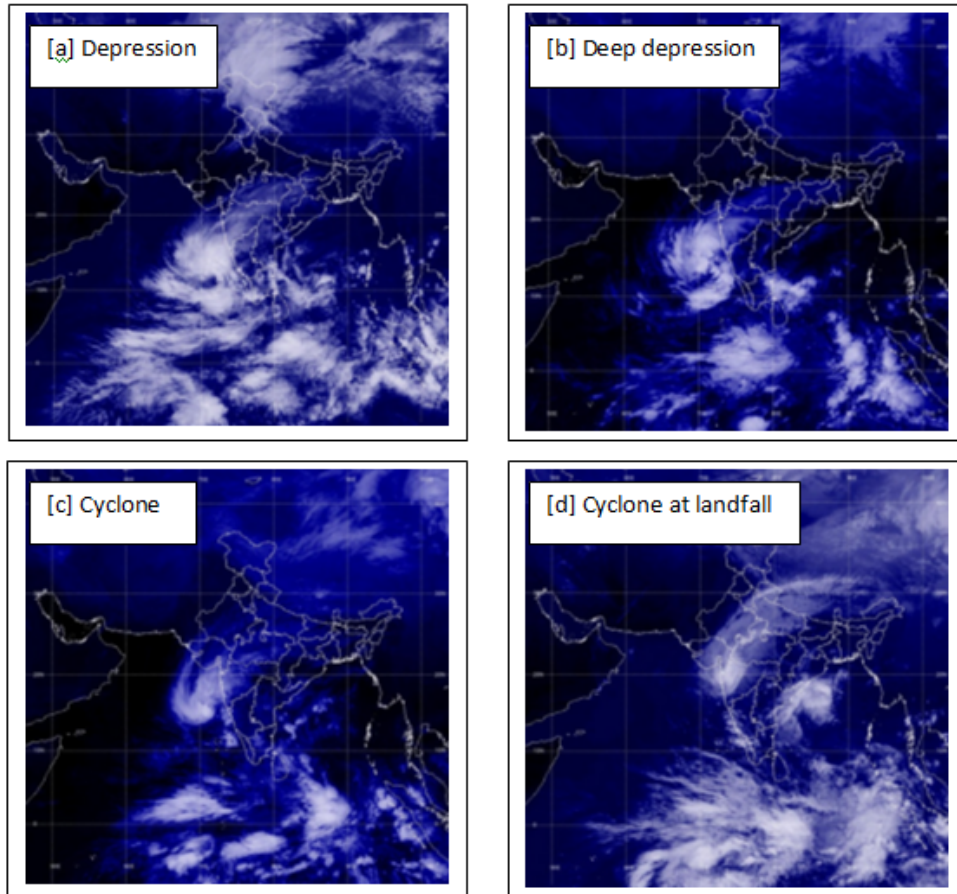


Fig. 1 INSAT Kalpana I satellite imageries of cyclonic storm *Phyan* at different stages of intensity (from IMD Report, November 2009).



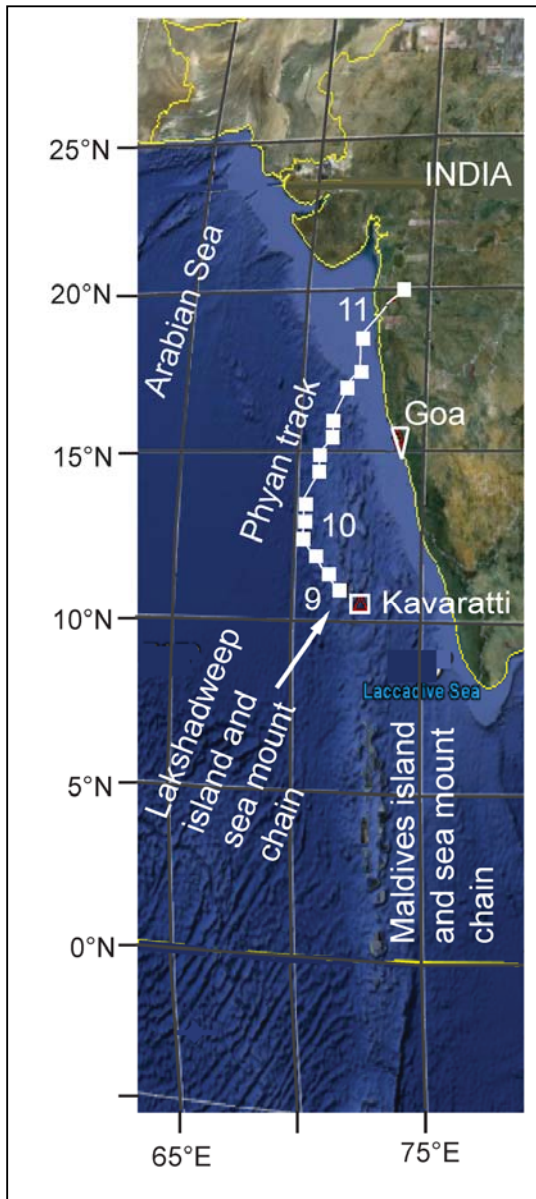


Fig. 2 Track of cyclonic storm *Phyan* during 09-12 November 2009 (from IMD Report, November 2009).

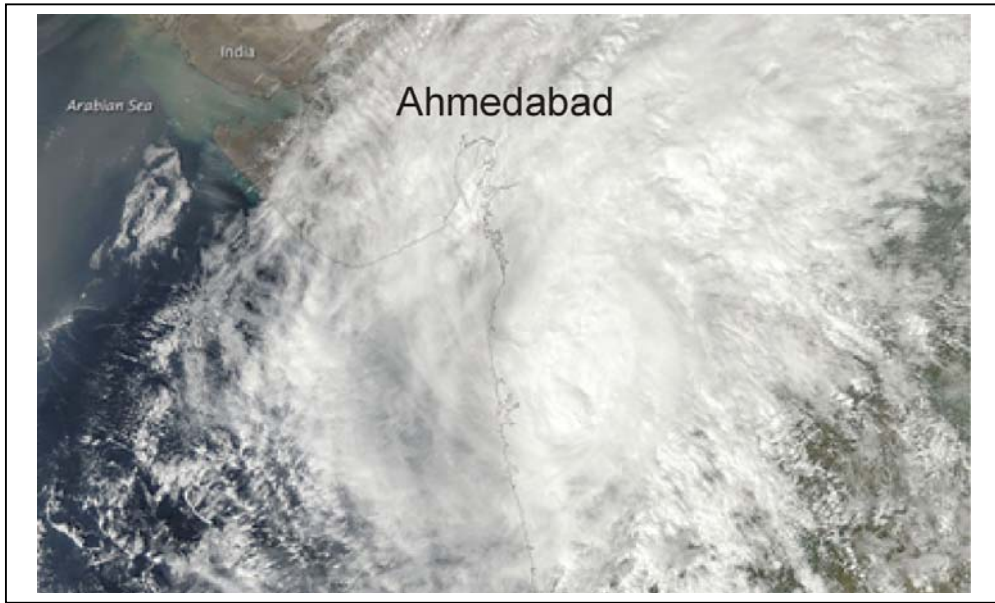


Fig. 3 NASA's Aqua satellite imagery of the spatial coverage of cyclonic storm *Phyan* (November 2009) over a large area on the west India region, stretching from the Arabian Sea toward the northeast over India's interior, blanketing much of the coast in clouds (Courtesy of National Aeronautics and Space Administration, USA).

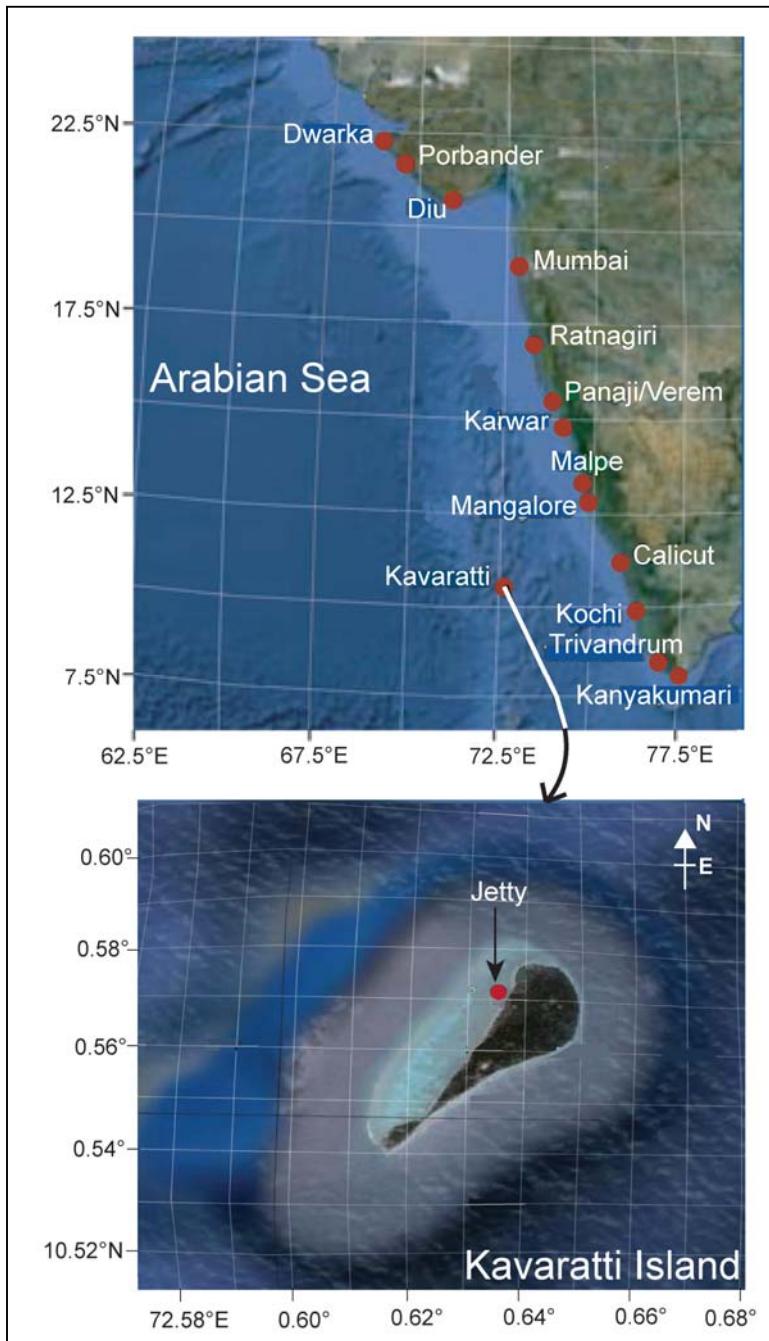


Fig. 4 Location map of measurement sites along the west coast of India and from Kavaratti Island region during the passage of tropical cyclone 'Phyan'.

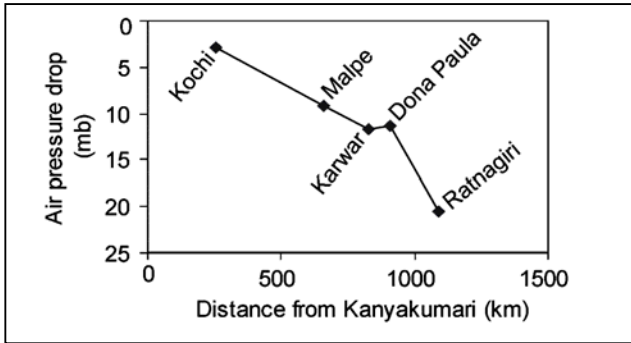


Fig. 5 Spatial distribution of barometric pressure drop along five west India coastal locations during the passage of Phyan

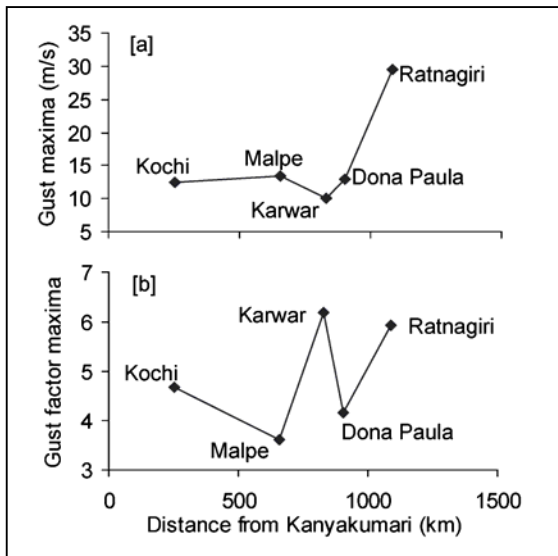


Fig. 6 Spatial distribution of [a] gust maxima and [b] gust factor maxima along five west India coastal locations during the passage of Phyan

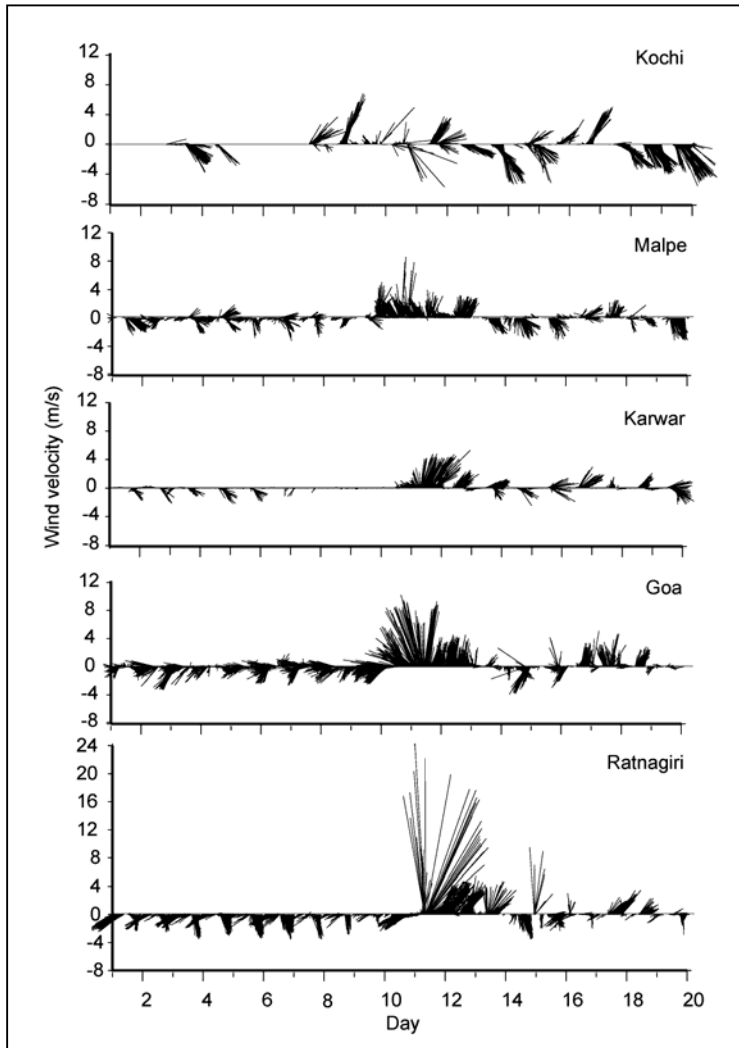


Fig. 7 Stick-plots of wind velocities at five west India coastal locations during the passage of Phyan during November 2009.

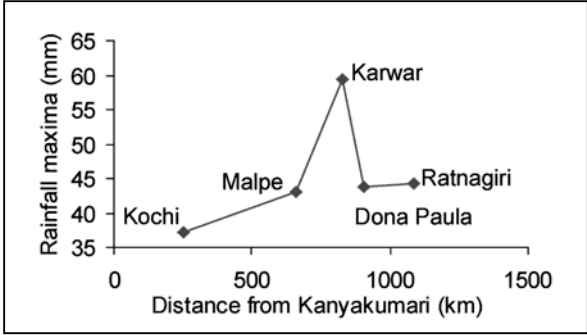


Fig. 8 Spatial distribution of 24-h cumulative rainfall maxima along five west India coastal waters during the passage of *Phyan*

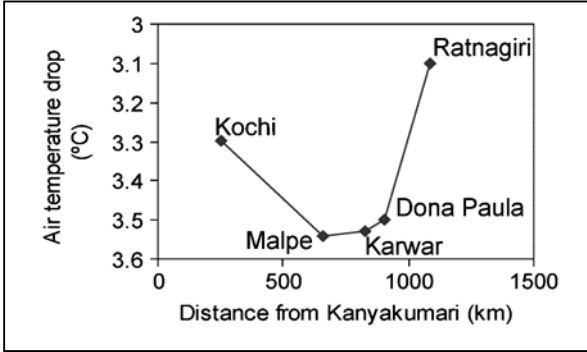


Fig. 9 Spatial distribution of air temperature drop along five west India coastal locations during the passage of *Phyan*

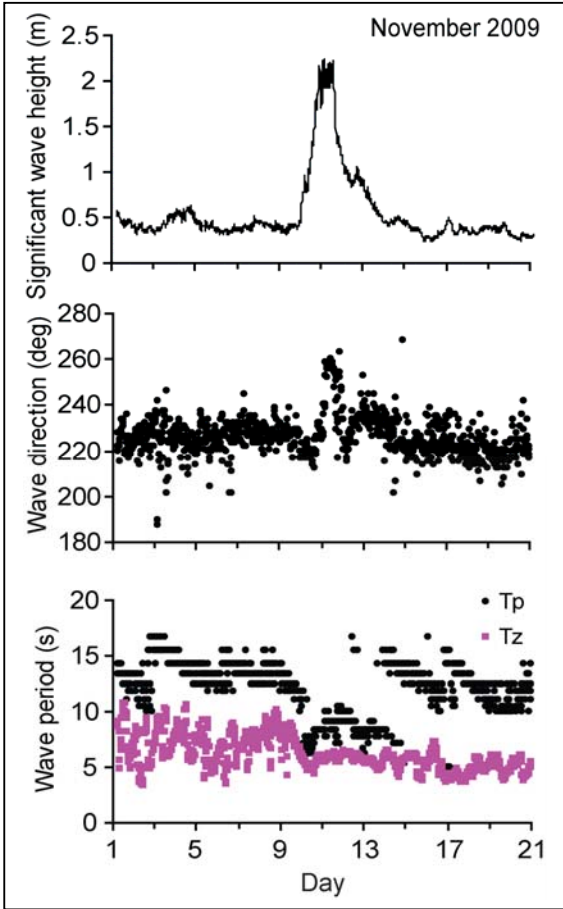


Fig. 10 Time series measurements of significant wave height, wave direction, peak wave period ( $T_p$ ) and mean wave period ( $T_z$ ) from Karwar made using directional wave rider buoy.

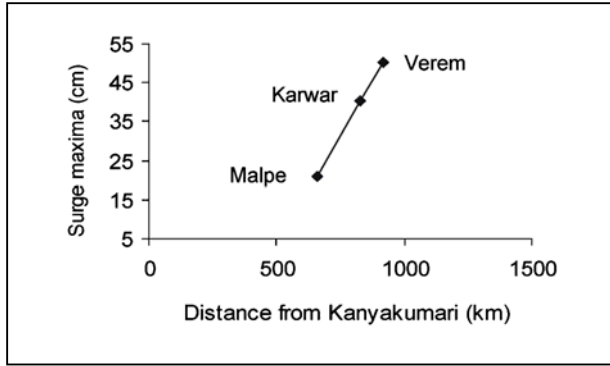


Fig. 11 Spatial distribution of surge maxima along three west India coastal locations during the passage of Phyan

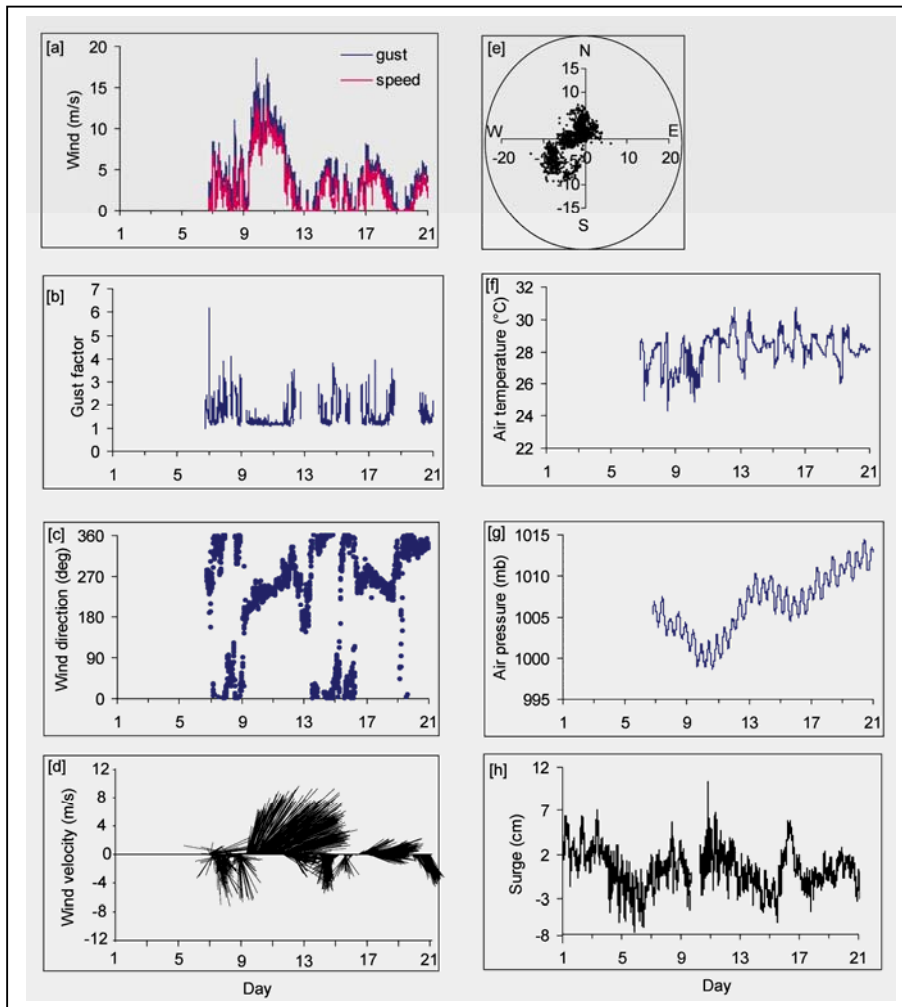


Fig. 12 In-situ measurements of the surface meteorological and storm surge features at the Kavaratti Island during the passage of Phyan; (a) wind speed and gust; (b) gust factor; . Wind speeds  $\geq 1$  m/s have been considered for estimation of gust factor; (c) wind direction; (d) stick plot of wind velocity; (e) scatter plot of wind speed; (f) air temperature; (g) air pressure; (h) surge.

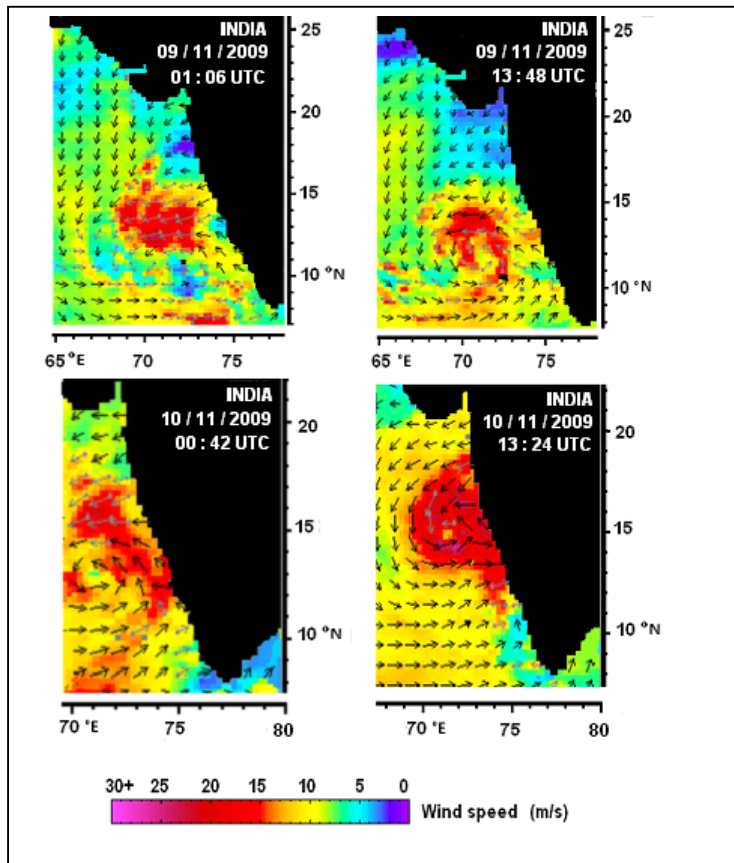


Fig. 13 Spatial structure and vortex motion of the wind field over the eastern Arabian Sea during the passage of Phyan (QuikSCAT satellite-derived vector plots)



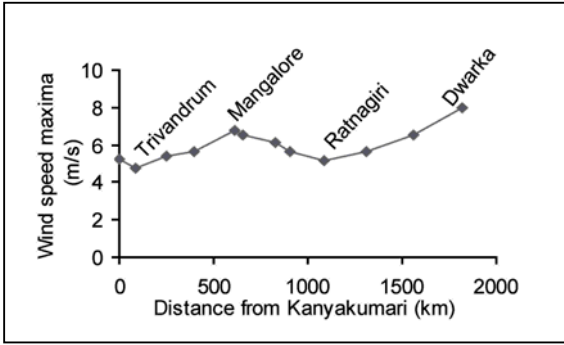


Fig. 14 Spatial distribution of the wind speed maxima along twelve west India coastal water locations during the passage of *Phyan*.

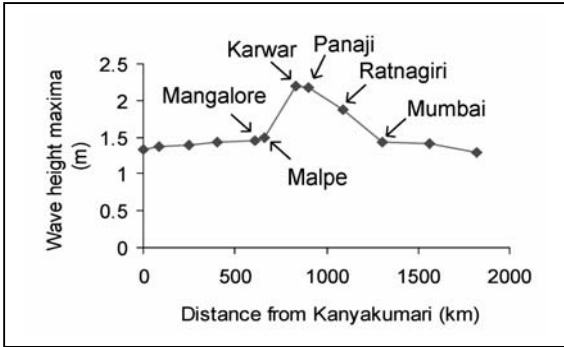


Fig. 15 Spatial distribution of significant wave height maxima along twelve west India coastal locations during the passage of *Phyan*.

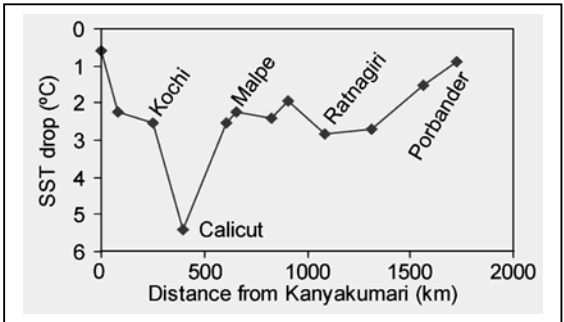


Fig. 16 Spatial distribution of SST drop along twelve west India coastal locations during the passage of *Phyan*.